Spontaneous instabilities and stick-slip motion in a generalized Hébraud–Lequeux model

Jean-Philippe Bouchaud, Stanislao Gualdi, Marco Tarzia, Francesco Zamponi

Spontaneous instabilities and stick-slip motion in a generalized Hébraud-Lequeux model

Jean-Philippe Bouchaud,[1] Stanislao Gualdi,[2] Marco Tarzia,[3] and Francesco Zamponi[4]

[1] *CFM, 23 rue de l'Université, 75007 Paris, France, and Ecole Polytechnique, 91120 Palaiseau, France.*
[2] *Laboratoire de Mathématiques Appliquées aux Systèmes, CentraleSupélec, 92290 Châtenay-Malabry, France*
[3] *Université Pierre et Marie Curie - Paris 6, Laboratoire de Physique Théorique de la Matière Condensée, 4, Place Jussieu, Tour 12, 75252 Paris Cedex 05, France*
[4] *Laboratoire de Physique Théorique, École Normale Supérieure, UMR 8549 CNRS, 24 Rue Lhomond, 75231 Paris Cedex 05, France*

We revisit the Hébraud-Lequeux (HL) model for the rheology of jammed materials and argue that a possibly important time scale is missing from HL's initial specification. We show that our generalization of the HL model undergoes interesting oscillating instabilities for a wide range of parameters, which lead to intermittent, stick-slip flows under constant shear rate. The instability we find is akin to the synchronization transition of coupled elements that arises in many different contexts (neurons, fireflies, financial bankruptcies, etc.). We hope that our scenario could shed light on the commonly observed intermittent, serrated flows of glassy materials under shear.

I. INTRODUCTION

Jammed materials are like Tolstoy's happy families: they all behave much in the same way. The (non-linear) rheological properties of very different materials such as metallic glasses, foams, dense emulsions or granular packings are remarkably similar. Typically, these materials flow very slowly below a certain yield stress, and exhibit interesting dynamical features such as "avalanches" [1, 2] (perhaps similar, at a different scale, to real earthquakes [3]) and intermittent, stick-slip like motion, which are still poorly understood – as is the transition from "liquid" flows to "jammed" flows [4]. At the microscopic scale all of these materials have very different properties and can barely be described by one single model. However on a more coarse grained level, when for example considering rheological or plasticity features, these materials show very similar properties. Such universality has motivated researchers to propose simple phenomenological models to account for them. It is now well accepted that the elementary physical process at play is the yielding of small regions of the material [5–13] (the so-called shear transformation zones, STZ), when the local shear stress exceeds some (possibly random) threshold. These STZ are localized but display long-range elastic interactions [14] that can trigger plastic instabilities. Among the most popular approaches to describe the stochastic collective evolution of these STZ is the Hébraud-Lequeux (HL) model [15], which is a very simple, mean-field description of the elastic interaction between such STZ, in particular how the instability of one of them can trigger the instability of many others (see also Refs. [16–20] for alternative descriptions and [21] for a recent review on this topic). The HL model, in spite of its simplicity, leads to highly non-trivial results, in particular a phase transition between a jammed, arrested phase and a liquid, flowing phase, with a non-linear Herschel-Bulkley law [22] for small shear rate in the jammed phase. This model has attracted a renewed interest in the recent years, focusing, inter-alia, on a detailed comparison with the competing Soft-Glassy-Rheology (SGR) models [23], on avalanche-like dynamics [24], and on a generalization of HL that appropriately accounts for the power-law decay of elastic interactions between STZ [25, 26], which deeply modifies the mathematical structure of the exact solution of the model.

In this paper, we revisit the original HL model and argue that some important physical time-scales are missing from its original formulation. Although many of the predictions of HL are unaffected by these modifications, we find that an oscillating instability can appear in some regions of parameter space. We find in particular that the "liquid" phase at zero shear rate is unstable and becomes, close enough the the jammed phase, spontaneously oscillating between a self-sustained liquid and a glass. This instability persists when the shear rate is weak enough, and leads, in physical terms, to an intermittent stick-slip flow (possibly related to so-called serrated flow). Interestingly, oscillatory instabilities also arise in some variants of the SGR models [27], or within simple phenomenological constitutive equations for shear-thickening materials [28]. However, the underlying physical mechanisms leading to instabilities are quite different from the one discussed in the present paper.

The intuition behind our instability in fact comes from a very similar model that we recently studied in the context of economic crisis "waves" and collective bank defaults [29, 30]. In all these cases, the common phenomenon is that the instability/default/bankruptcy of a single element can trigger the instabilities of others through interactions. The somewhat surprising feature, however, in that such a coupling can lead to the synchronization of randomly evolving entities, and genuine oscillations – see [30, 31] and references therein.

The outline of the paper is as follows: we first gener-

alize the HL model such as to describe more accurately what happens when a single entity fails. We then show that the zero shear stationary state computed by HL is linearly unstable to some oscillatory mode in a region of parameters, in particular close to the jamming transition. We then extend our calculation to non-zero shear rates and find the "phase diagram" of the model, in particular we highlight the region where stick-slip motion is expected. We finally conclude and discuss possible extensions of our calculations.

II. THE MODEL

Let us recall the basic tenets of the HL model [15] and introduce the physical items that we believe are missing from the original framework. Following HL, the material is divided in N regions (or "elements") labeled by an index $i = 1, \cdots, N$, each characterized by a local stress σ_i. The stress σ_i of each element performs a random walk with:

- a drift $G_0\dot{\gamma}$ due to the external shear $\dot{\gamma}$ that loads elastic energy (G_0 is the elastic shear modulus),
- a time-dependent diffusion D_t due to intrinsic noise and elastic interactions between elements.

Whenever $|\sigma_i| \geq \sigma_c$, the i-th element may become unstable, and becomes so at a "plastic" rate $1/\tau_{\rm pl}$. As soon as the element becomes unstable (it is then in a "fluid" state), HL postulates that it re-jams (with $\sigma = 0$) immediately in a state of zero stress. We rather assume that it remains in its fluid state during a typical time scale $\tau_{\rm fl}$; in such a state, the element cannot contribute to the shear stress (see also Fig. 1 in Ref. [32], where $\tau_{\rm fl}$ has been called $\tau_{\rm el}$). With rate $1/\tau_{\rm fl}$, the element re-jams with $\sigma = 0$, as in HL.[1] This is a very important ingredient for a correct physical interpretation of the model [18, 32]: note that once an element becomes unstable, its dynamics cannot be described by the same drift-diffusion mechanism. On the contrary, when an element becomes unstable, it contributes to the total plastic activity at time t, called Γ_t, and increases the diffusion of all other elements identically, in a mean-field way, exactly as in the HL model (see [25] for an improved description). However, we will assume that the plastic activity at time t affects the diffusion coefficient D_t with some delay, instead of instantaneously as HL assumed. This reflects, at the mean-field level, the finite propagation speed of information through the sample.

[1] This could actually be generalized to the case where the stress drops to a finite fraction of the initial stress (as in [33]), or to a non-trivial distribution of initial stresses; the instability reported below survives provided the width of that distribution remains small.

A. Mathematical definition of the model

Our modified model can be described by the same Fokker-Planck setting as used by HL [15]. The evolution of the (unnormalized[2]) probability $P(\sigma, t)$ to find an element with stress σ at time t is given by:

$$\begin{aligned} \dot{P}(\sigma,t) &= D_t P''(\sigma,t) - G_0\dot{\gamma}P'(\sigma,t) \\ &\quad + J_t\delta(\sigma) - \frac{1}{\tau_{\rm pl}}P(\sigma,t)H(|\sigma|-\sigma_c) \ , \end{aligned} \tag{1}$$

where $H(x)$ is the Heaviside step function, and with:

$$\begin{aligned} J_t &= \frac{1}{\tau_{\rm fl}}(1-\phi_t) \ , \\ \phi_t &= \int_{-\infty}^{\infty} d\sigma \, P(\sigma,t) \ , \\ \Gamma_t &= \frac{1}{\tau_{\rm pl}}\int_{|\sigma|\geq\sigma_c} d\sigma \, |\sigma| P(\sigma,t) \ , \\ D_t &= D_{\rm int} + \alpha\omega\int_{-\infty}^{t} ds \ e^{-\omega(t-s)}\Gamma_s \ . \end{aligned} \tag{2}$$

Here, ϕ_t is the fraction of jammed elements that contribute to the elastic stress and J_t is the flux of elements that re-jam between t and $t + {\rm d}t$, initially at zero stress. The fraction of fluidized elements, $(1-\phi_t)$, contributes a viscous stress proportional to $\dot{\gamma}$. Hence, the total stress is

$$\Sigma_t = \int_{-\infty}^{\infty} d\sigma \, \sigma \, P(\sigma,t) + (1-\phi_t)\eta\dot{\gamma} \ , \tag{3}$$

where η is the microscopic viscosity of the fluid elements. Note that ϕ_t satisfies the equation:

$$\dot{\phi}_t = \frac{1}{\tau_{\rm fl}}(1-\phi_t) - \frac{1}{\tau_{\rm pl}}\int_{|\sigma|\geq\sigma_c} d\sigma P(\sigma,t) \ . \tag{4}$$

The equation for D_t means that yielding events, when they happen, impose an extra random stress onto other elements but with some time lag that we model as an exponential kernel, with a coupling constant α. $D_{\rm int}$ is an intrinsic noise term (for example temperature) that we will choose to be very small in the following. Furthermore we choose $G_0 = 1$ without loss of generality. The control parameters for this model are $\sigma_c, \dot{\gamma}, \tau_{\rm fl}, \tau_{\rm pl}, D_{\rm int}, \alpha, \omega$. Because one can fix arbitrarily the units of σ and of t, there are in fact four plus one independent adimensional control parameters: for example $\widehat{\gamma} := \dot{\gamma}\tau_{\rm fl}/\sigma_c$, α, $\tau_{\rm pl}/\tau_{\rm fl}$, $\widehat{\omega} := \omega\tau_{\rm fl}$, and finally ${\rm Pe} := \dot{\gamma}\sigma_c/D_{\rm int} \to \infty$ throughout this paper.

[2] The reason why $P(\sigma,t)$ is not normalised is that it does not include the fraction $(1-\phi_t)$ of elements that are in the fluid state, see Eq. (2).

B. Connection with the Hébraud-Lequeux model

The standard HL model is recovered if we set $D_{\rm int} = 0$, $\tau_{\rm fl} = 0$ and $\omega = \infty$, i.e: no intrinsic noise, fluid regions re-jam instantaneously, and yielding elements affect the stress of other regions instantaneously as well. In the HL limit $\tau_{\rm fl} = 0$, we therefore have $\dot{\phi}_t = 0$ and $\phi_t \equiv 1$, and from Eq. (4) we have $J_t = \frac{1}{\tau_{\rm pl}} \int_{|\sigma|\geq\sigma_c} d\sigma P(\sigma, t)$. For $D_{\rm int} = 0$ and $\omega \to \infty$, we indeed recover HL's prescription $D_t = \alpha\Gamma_t$. Summarizing, we obtain Eq. (1) with

$$\begin{aligned} J_t &= \frac{1}{\tau_{\rm pl}} \int_{|\sigma|\geq\sigma_c} d\sigma P(\sigma, t) \ , \\ D_t = \alpha\Gamma_t &= \frac{\alpha}{\tau_{\rm pl}} \int_{|\sigma|\geq\sigma_c} d\sigma |\sigma| P(\sigma, t) \ . \end{aligned} \tag{5}$$

This coincides with the HL model, with the only difference that Γ_t is defined without the $|\sigma|$. Although this does not make any important difference in the properties of the model, in particular the instability described below, we argue that our definition has a more precise physical interpretation, since the plastic activity should be the average of $|\sigma|$. In conclusion, the presence of the additional time scales $\tau_{\rm fl}$ and $1/\omega$ is the main difference between our model and HL, and we will see that they play a crucial role in the physics of the model.

C. The limit $\tau_{\rm pl} \to 0$

For the ease of analytical calculations, we will set in the following $\tau_{\rm pl} = 0$, which means that an element becomes unstable immediately when $|\sigma| > \sigma_c$, while keeping a finite fluid lifetime $\tau_{\rm fl}$. The HL model corresponds to $\tau_{\rm pl}/\tau_{\rm fl} \to \infty$, but the limit $\tau_{\rm pl}/\tau_{\rm fl} \ll 1$ looks more physical to us, and will lead to an oscillating instability, which disappears when $\tau_{\rm pl}/\tau_{\rm fl}$ exceeds a (parameter dependent) threshold value, simply because the synchronisation effect reported below cannot set in. So strictly speaking, the instability reported here is absent in the original HL setting.

When $\tau_{\rm pl} = 0$, Eq. (1) is simply complemented by an absorbing boundary condition at $|\sigma| = \sigma_c$, implying $P(|\sigma| = \sigma_c) = 0$. Furthermore, the plastic activity is given by the number of regions that become unstable per unit time, hence in Eq. (2) Γ_t is given by the outgoing flux at $\pm\sigma_c$, i.e.:

$$\Gamma_t = \sigma_c D_t [P'(-\sigma_c, t) - P'(\sigma_c, t)] \ . \tag{6}$$

Note that in this limit the difference in our definition of Γ_t with respect to HL becomes irrelevant, because $|\sigma| = \sigma_c$ is the only contribution to Γ_t. For simplicity, we also set $\sigma_c = 1$ in the following.

III. VANISHING SHEAR RATE

We will consider first the situation with no external shear, i.e. $\dot{\gamma} = 0$. It turns out that the interesting limit corresponds to the case when the intrinsic activity tends to zero, i.e. $D_{\rm int} \to 0$, as in the HL model. The only two adimensional control parameters left are thus α and $\widehat{\omega} := \omega\tau_{\rm fl}$.

A. The stationary solution: a jamming transition

We first look for a stationary solution of Eq. (1) with $P(\sigma, t) = P_0(\sigma)$, $J_t = J_0$, etc., which in this case is particularly simple and reads:

$$P_0(\sigma > 0) = A(1 - \sigma) \ , \qquad P_0(-\sigma) = P_0(\sigma) \ , \tag{7}$$

with the discontinuity of the slope at the origin related to J_0 by Eq. (1) as $2D_0A = J_0$. The fraction of active elements $\phi_0 = \int_{-1}^{1} d\sigma P_0(\sigma)$ is simply given by A, so that from Eq. (2)

$$J_0 = \frac{1}{\tau_{\rm fl}}(1 - A) \quad \longrightarrow \quad A = \frac{1}{2D_0\tau_{\rm fl} + 1} \ . \tag{8}$$

Eq. (6) gives $\Gamma_0 = 2AD_0$ and from Eq. (1) we get $D_0 = D_{\rm int} + \alpha\Gamma_0 = D_{\rm int} + 2\alpha AD_0$. We thus obtain a self-consistent equation for the stationary value of the diffusion coefficient

$$2D_0^2\tau_{\rm fl} + D_0(1 - 2\alpha - 2D_{\rm int}\tau_{\rm fl}) - D_{\rm int} = 0 \ . \tag{9}$$

This second degree equation has two possible solutions that read, in the limit $D_{\rm int} \to 0$:

$$D_0^- = \frac{D_{\rm int}}{1 - 2\alpha} \ ; \qquad D_0^+ = \frac{2\alpha - 1}{2\tau_{\rm fl}} - \frac{\alpha D_{\rm int}\tau_{\rm fl}}{2(1 - 2\alpha)} \ , \tag{10}$$

where clearly the first solution holds for $\alpha < 1/2$ and the second holds for $\alpha > 1/2$. When $D_{\rm int} \to 0$ there is, as first noted by HL, a transition between a fluid phase $\alpha > 1/2$ where activity is self sustained $D_0^+ > 0$, and a jammed phase $\alpha < 1/2$ where activity is absent, $D_0^- = 0$, see Fig. 1 and Ref. [23]. In the jammed phase, one has $A = 1$ and in the liquid phase, $A = 1/(2\alpha)$, to leading order in $D_{\rm int}$.

B. Linear stability analysis

Following [30], we are interested in studying the stability of the stationary solution with respect to a linear perturbation. We thus write $P(\sigma, t) = P_0(\sigma) + \varepsilon P_1(\sigma, t)$, $D_t = D_0 + \varepsilon D_1(t)$, $\phi_t = \phi_0 + \varepsilon\phi_1(t)$. Linearizing Eq. (1) we get

$$\dot{P}_1(\sigma, t) = D_0 P_1''(\sigma, t) + D_1(t) P_0''(\sigma) - \frac{1}{\tau_{\rm fl}}\phi_1(t)\delta(\sigma) \ , \tag{11}$$

with the boundary conditions $P_1(\sigma = \pm 1, t) = 0$. Therefore,

$$P_1(\sigma,t) = \int_0^\infty d\tau \int_{-1}^{1} d\bar{\sigma}\, G(\sigma,t|\bar{\sigma},t-\tau) \times \left[D_1(t-\tau) P_0''(\bar{\sigma}) - \frac{1}{\tau_{\rm fl}} \phi_1(t-\tau)\delta(\bar{\sigma}) \right] . \tag{12}$$

where $P_0''(\sigma) = -2A\delta(\sigma)$, and G is the random walk propagator in the interval $[-1,+1]$.

Combining Eqs. (2) and (6), setting $D_{\rm int} = 0$ in the linear regime we obtain an equation for the diffusion constant $D_1(t)$:

$$D_1(t) = \alpha\omega \int_{-\infty}^{t} ds D_0 \left[P_1'(-1,s) - P_1'(1,s) \right] e^{-\omega(t-s)} + 2A\alpha\omega \int_{-\infty}^{t} ds D_1(s) e^{-\omega(t-s)} . \tag{13}$$

Exponentials of time, with $D_1(t) = \mathcal{D}e^{\lambda t}$, $\phi_1(t) = \Phi e^{\lambda t}$, $P_1'(-1,t) = -P_1'(1,t) = \Pi e^{\lambda t}$, are consistent solutions of the linearized equations. We find from Eq. (13):

$$\mathcal{D} = \frac{2\alpha\omega D_0}{\omega(1-2\alpha A) + \lambda} \Pi . \tag{14}$$

In order to compute $P_1(\sigma,t)$ simply, one can notice that $H_{\bar{\sigma}}(\sigma,\lambda) = \int_0^\infty d\tau e^{-\lambda\tau} G(\sigma,\tau|\bar{\sigma},0)$ obeys the following partial differential equation:

$$D_0 H_{\bar{\sigma}}''(\sigma,\lambda) - \lambda H_{\bar{\sigma}}(\sigma,\lambda) = -\delta(\sigma - \bar{\sigma}) , \tag{15}$$

with boundary condition $H_{\bar{\sigma}}(\sigma = \pm 1, \lambda) = 0$. Specializing to $\bar{\sigma} = 0$, one finds:

$$H(\sigma > 0, \lambda) = \widehat{A} \left[e^{-\kappa\sigma} - e^{-2\kappa} e^{\kappa\sigma} \right] , \quad H(-\sigma,\lambda) = H(\sigma,\lambda) \tag{16}$$

with $\kappa^2 = \lambda/D_0$. The discontinuity of the first derivative at the origin gives:

$$2D_0 \widehat{A} = \frac{1}{\kappa(1+e^{-2\kappa})} , \tag{17}$$

so finally $H'(-1,\lambda) = -H'(1,\lambda) = 1/(2D_0 \cosh\kappa)$. Plugging this in the general expression for $P_1(\sigma,t)$ in Eq. (12), taking the derivative with respect to σ and setting $\sigma = -1$ finally leads to:

$$\Pi = -\frac{1}{2D_0 \cosh\kappa} \left[2A\mathcal{D} + \frac{1}{\tau_{\rm fl}} \Phi \right] . \tag{18}$$

Finally, integrating Eq. (11) over σ leads to:

$$\lambda\Phi = -\frac{1}{\tau_{\rm fl}} \Phi - 2D_0 \Pi - 2\mathcal{D}A . \tag{19}$$

In the liquid phase ($D_0 > 0$ and $A = 1/(2\alpha)$) the solvability condition of the system of Eqs. (14), (18), (19) relating $\mathcal{D}, \Pi$ and Φ finally reads, in terms of $\widehat{\lambda} = \lambda\tau_{\rm fl}$ and $\widehat{\omega} = \omega\tau_{\rm fl}$:

$$1 + \widehat{\lambda} = \frac{\widehat{\omega} + \widehat{\lambda}}{\widehat{\omega} + \widehat{\lambda} \cosh \sqrt{\frac{\widehat{\lambda}}{\alpha - 1/2}}} , \tag{20}$$

or equivalently (for $\widehat{\lambda} \neq 0$)

$$\widehat{\omega} = 1 - (1+\widehat{\lambda}) \cosh \sqrt{\frac{\widehat{\lambda}}{\alpha - 1/2}} . \tag{21}$$

If all the solutions of Eq. (21) have a negative real part, the stationary solution is stable, while it is unstable otherwise. This condition defines the transition point $\alpha_{\rm c}(\widehat{\omega})$. Note that for $\alpha \to \infty$ we obtain from Eq. (21) that $\widehat{\lambda} = -\widehat{\omega}$ and therefore the stationary state is stable.

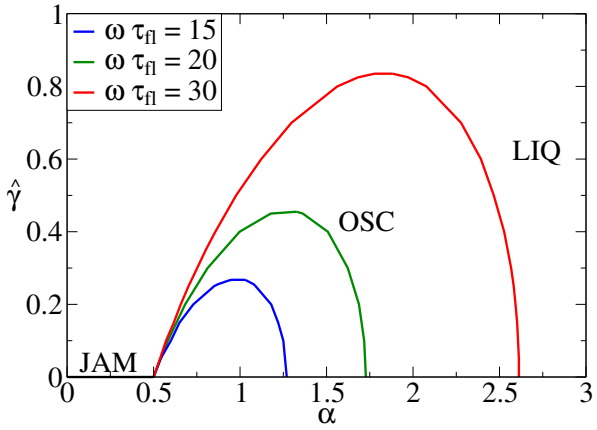

FIG. 1: Phase diagram of the model in the $(\alpha, \widehat{\gamma})$ plane (recall that $\widehat{\gamma} = \dot{\gamma}\tau_{\rm fl}$) obtained from the solutions of Eq. (40) with $D_i \to 0$ and different values of $\widehat{\omega} = \omega\tau_{\rm fl}$.

C. Large ω analysis

Eq. (21) can be analyzed in the limit of large ω (that corresponds to the HL case where stress propagation is instantaneous throughout the sample), assuming that $\alpha_{\rm c}(\widehat{\omega})$ and $\widehat{\lambda}$ are also large (we will see that they are proportional to $\widehat{\omega}$). We obtain

$$\widehat{\omega} = -\widehat{\lambda} \cosh \sqrt{\frac{\widehat{\lambda}}{\alpha}} . \tag{22}$$

Let us assume that at the transition there is a single unstable mode whose real part crosses zero continuously. Thus $\widehat{\lambda} = i\lambda_{\rm I}$ is pure imaginary at $\alpha_{\rm c}$. In this case, for the r.h.s. of Eq. (22) to be real we need $\cos\sqrt{\lambda_{\rm I}/(2\alpha)} = 0$ which implies $\lambda_{\rm I} = \alpha\pi^2(1+2n)^2/2$ with $n \in \mathbb{Z}$. Then we get

$$\frac{\widehat{\omega}}{\alpha} = (-1)^n \frac{\pi^2}{2} (1+2n)^2 \sinh\left(\frac{\pi}{2}(1+2n) \right) . \tag{23}$$

Because the system is stable at $\alpha \to \infty$, the stability boundary corresponds to the largest value of α for which a mode is unstable, and thus to the smallest value of the r.h.s. of Eq. (23), which is assumed for $n = 0$ and gives

$$\frac{\alpha_c(\widehat{\omega})}{\widehat{\omega}} = \frac{2}{\pi^2 \sinh\left(\frac{\pi}{2}\right)} = 0.088055\ldots \ , \qquad (24)$$

in excellent agreement with the numerical results of Fig. 1 when $\widehat{\omega}$ is large enough (for example, $\widehat{\omega} = 30$ should correspond to $\alpha_c \approx 2.64$).

D. Summary

Let us summarize the content of this section. We discussed the case of vanishing shear rate, $\dot{\gamma} = 0$, and intrinsic activity, $D_{\rm int} \to 0$, assuming $\tau_{\rm pl} \ll \tau_{\rm fl}$. The control parameters are α and $\widehat{\omega} = \omega\tau_{\rm fl}$. We found that:

- For $\alpha < 1/2$, the system is jammed: no motion occurs as $D_t \equiv 0$.
- For $\alpha > \alpha_c(\widehat{\omega}) \approx \widehat{\omega} \times 0.088055\ldots$, there is a stationary "liquid" phase with self-sustained activity, $D_t \equiv D_0 > 0$.
- For $1/2 < \alpha < \alpha_c(\widehat{\omega})$ the liquid phase is in fact unstable; in this case, as shown in Fig. 2, the system undergoes spontaneous oscillations between periods where the number of fluid elements is large and periods where it is small. When an external shear is applied, this state will correspond to intermittent, stick-slip motion.

Let us emphasize that the liquid phase of the model is unphysical in the strict limit $D_{\rm int} = 0$ and $\dot{\gamma} = 0$, because no motion is possible in this case. However, one can think that $D_{\rm int}$ is very small but finite, modeling some external noise (e.g. a small temperature), or that $\dot{\gamma} \to 0^+$. As we discuss next, the more interesting case $\dot{\gamma} > 0$ is indeed perfectly regular in the limit where $\dot{\gamma} \to 0$.

IV. NON-ZERO SHEAR RATE

We now generalize the calculation to a non-zero external shear, $\dot{\gamma} \neq 0$, still in the limit $D_{\rm int} \to 0$. In addition to α and $\widehat{\omega} = \omega\tau_{\rm fl}$, there is now a third control parameter $\widehat{\gamma} = \dot{\gamma}\tau_{\rm fl}$. We also define $\zeta = \dot{\gamma}\sigma_c/D_0$, which is an adimensional "renormalized Péclet number" quantifying the importance of drift with respect to the steady-state diffusion constant in Eq. (1). Remember however that we set $\sigma_c = 1$ henceforth.

A. The static case

The stationary solution now reads:

$$\begin{aligned} P_0(\sigma > 0) &= A(1 - e^{-\zeta(1-\sigma)}) \ , \\ P_0(\sigma < 0) &= -Ae^{-\zeta}(1 - e^{\zeta(1+\sigma)}) \ . \end{aligned} \qquad (25)$$

Integrating Eq. (1) one can relate the discontinuity of the slope at the origin to J_0 as $A = \frac{J_0}{\dot{\gamma}} \frac{1}{1+e^{-\zeta}}$. Moreover, the fraction of active elements is $\phi_0 = A(1 - e^{-\zeta})$, and $J_0 = (1 - \phi_0)/\tau_{\rm fl}$. We thus have three equations for J_0, ϕ_0 and A and the solution is

$$J_0 = \frac{\dot{\gamma}}{\dot{\gamma}\tau_{\rm fl} + \tanh(\zeta/2)} \ , \qquad (26)$$

from which we obtain ϕ_0 and A thus completing the calculation of $P_0(\sigma)$.

From $P_0(\sigma)$ we obtain the self-consistent equation obeyed by $D_0 = \dot{\gamma}/\zeta$. Combining Eqs. (2) and (6), we have $D_0 = D_{\rm int} + \alpha\Gamma_0 = D_{\rm int} + \alpha D_0[P_0'(-1) - P_0'(1)]$. For $D_{\rm int} \to 0$ we obtain:

$$\frac{D_0}{\dot{\gamma}} = \frac{1}{\zeta} = \frac{\alpha}{\widehat{\gamma} + \tanh(\zeta/2)} \ . \qquad (27)$$

One is now always in a "liquid" phase with a finite diffusion constant $D_0 > 0$, induced by the shear rate. However, the dependence on $\dot{\gamma}$ is very different when $\alpha > 1/2$ or when $\alpha < 1/2$. For $\alpha \leq 1/2$, one indeed finds that ζ is finite for $\dot{\gamma} \to 0$, and satisfies $\tanh(\zeta/2)/\zeta = \alpha$; D_0 then behaves as $\dot{\gamma}$ when $\dot{\gamma} \to 0$. For $\alpha > 1/2$ instead, D_0 has a finite limit given by $D_0 = D_0^+ = (2\alpha - 1)/(2\tau_{\rm fl})$ for $\dot{\gamma} \to 0$, as in Eq. (10). Note that $\zeta \to 0$ for $\alpha \to 1/2^-$. Thus $D_0 = D_0^+ + O(\dot{\gamma}^2)$ for $\alpha > 1/2$ – see also [23].

B. Linear stability analysis

We linearize once again Eq. (1) with $P(\sigma, t) = P_0(\sigma) + \varepsilon P_1(\sigma, t)$, $D_t = D_0 + \varepsilon D_1(t)$, $\phi_t = \phi_0 + \varepsilon\phi_1(t)$. The linearized equation reads:

$$\begin{aligned} \dot{P}_1(\sigma, t) = D_0 P_1''(\sigma, t) - \dot{\gamma} P_1'(\sigma, t) \\ + D_1(t) P_0''(\sigma) - \frac{1}{\tau_{\rm fl}} \phi_1(t)\delta(\sigma) \ , \end{aligned} \qquad (28)$$

with the boundary conditions $P_1(\sigma = \pm 1, t) = 0$. Therefore

$$\begin{aligned} P_1(\sigma, t) = \int_0^\infty d\tau \int_{-1}^1 d\bar{\sigma}\, G_{\dot{\gamma}}(\sigma, t|\bar{\sigma}, t - \tau) \\ \times \left[D_1(t - \tau) P_0''(\bar{\sigma}) - \frac{1}{\tau_{\rm fl}} \phi_1(t - \tau)\delta(\bar{\sigma}) \right] \ , \end{aligned} \qquad (29)$$

where $G_{\dot\gamma}$ is the biased random walk propagator in the interval $[-1,+1]$. The diffusion constant $D_1(t)$ satisfies:

$$D_1(t) = \alpha\omega \int_{-\infty}^{t} ds D_0 \left[P_1'(-1,s) - P_1'(1,s)\right] e^{-\omega(t-s)} + \frac{J_0}{D_0}\alpha\omega \int_{-\infty}^{t} ds D_1(s) e^{-\omega(t-s)} \ . \tag{30}$$

Assuming exponential (in time) solutions with $D_1(t) = \mathcal{D}e^{\lambda t}$, $\phi_1(t) = \Phi e^{\lambda t}$, $P_1'(\pm 1,t) = \mp\Pi_\pm e^{\lambda t}$, we find from Eq. (30):

$$\mathcal{D} = \frac{\alpha\omega D_0}{\omega(1-\alpha J_0/D_0)+\lambda}(\Pi_+ + \Pi_-) \ . \tag{31}$$

Integrating Eq. (28) over α and using $P_1(\sigma=\pm1,t)=0$ leads to:

$$\lambda\Phi = -\frac{1}{\tau_{\rm fl}}\Phi - D_0(\Pi_+ + \Pi_-) - \mathcal{D}\frac{J_0}{D_0} \ . \tag{32}$$

In order to compute $P_1(\sigma,t)$ simply, one can notice that $H_{\bar\sigma}(\sigma,\lambda;\dot\gamma) = \int_0^\infty d\tau e^{-\lambda\tau} G_{\dot\gamma}(\sigma,\tau|\bar\sigma,0)$ obeys the following equation:

$$D_0 H''_{\bar\sigma}(\sigma,\lambda;\dot\gamma) - \dot\gamma H'_{\bar\sigma}(\sigma,\lambda;\dot\gamma) - \lambda H_{\bar\sigma}(\sigma,\lambda;\dot\gamma) = -\delta(\sigma-\bar\sigma) \ ,$$

with boundary condition $H_{\bar\sigma}(\sigma=\pm1,\lambda;\dot\gamma)=0$. We will denote $\kappa_\pm$ the two real roots of the equation:

$$D_0\kappa^2 - \dot\gamma\kappa - \lambda = 0 \ , \tag{33}$$

and $\Delta = \kappa_+ - \kappa_-$. The solution then reads, respectively for $\sigma > \bar\sigma$ and $\sigma < \bar\sigma$:

$$H_{\bar\sigma}(\sigma,\lambda;\dot\gamma) = A_\pm(\bar\sigma)e^{\kappa_+\sigma} + B_\pm(\bar\sigma)e^{\kappa_-\sigma} \ , \tag{34}$$

with the following equations coming from boundary conditions:

$$\begin{aligned} &A_\pm e^{\pm\kappa_+} = -B_\pm e^{\pm\kappa_-} \Rightarrow B_\pm = -A_\pm e^{\pm\Delta} \ , \\ &(A_+ - A_-)e^{\kappa_+\bar\sigma} + (B_+ - B_-)e^{\kappa_-\bar\sigma} = 0 \ , \\ &\kappa_+(A_+ - A_-)e^{\kappa_+\bar\sigma} + \kappa_-(B_+ - B_-)e^{\kappa_-\bar\sigma} = -\frac{1}{D_0} \ . \end{aligned} \tag{35}$$

Solving for $A_\pm$ yields:

$$A_\pm(\bar\sigma) = \frac{e^{\mp\Delta-\kappa_+\bar\sigma} - e^{-\kappa_-\bar\sigma}}{2D_0\Delta\sinh\Delta}. \tag{36}$$

The relevant quantities here are $H'_{\bar\sigma}(\sigma=\pm1,\lambda;\dot\gamma)$, which are expressed as:

$$\begin{aligned} H'_{\bar\sigma}(\sigma=\pm1,\lambda;\dot\gamma) &= \kappa_+ A_\pm(\bar\sigma)e^{\pm\kappa_+} + \kappa_- B_\pm(\bar\sigma)e^{\pm\kappa_-} \\ &= A_\pm(\bar\sigma)\Delta e^{\pm\kappa_+} \ . \end{aligned}$$

Using

$$\begin{aligned} &D_0 P_0''(\sigma) = \dot\gamma P_0'(\sigma) - J_0\delta(\sigma) \ , \\ &P_0'(\sigma>0) = -A\zeta e^{-\zeta(1-\sigma)}, \qquad P_0'(\sigma<0) = A\zeta e^{\zeta\sigma} \ , \end{aligned}$$

in Eq. (29), one finds two contributions. The one coming from $\delta(\bar\sigma)$ reads:

$$\Pi_\pm^\delta = \pm\left(\frac{J_0\mathcal{D}}{D_0} + \frac{1}{\tau_{\rm fl}}\Phi\right)\frac{e^{\pm\kappa_-} - e^{\pm\kappa_+}}{2D_0\sinh\Delta} \ , \tag{37}$$

while the continuous part gives:

$$\Pi_\pm^c = \mp\frac{\dot\gamma\mathcal{D}}{D_0}\Delta e^{\pm\kappa_+}\int_{-1}^{+1} {\rm d}\bar\sigma P_0'(\bar\sigma)A_\pm(\bar\sigma) \ . \tag{38}$$

From these we deduce:

$$\begin{aligned} \Pi_+^\delta + \Pi_-^\delta &= \left(\frac{J_0\mathcal{D}}{D_0} + \frac{1}{\tau_{\rm fl}}\Phi\right)\frac{\sinh\kappa_- - \sinh\kappa_+}{D_0\sinh\Delta} \ , \\ \Pi_+^c + \Pi_-^c &= -\frac{J_0\mathcal{D}\zeta}{D_0^2\kappa_+\kappa_-}\frac{(e^{-\kappa_+}-1)(e^{-\kappa_-}-1)}{e^{-\zeta}+1}\times \\ &\quad\times\frac{\kappa_+\sinh\kappa_- - \kappa_-\sinh\kappa_+}{\sinh\Delta} \ . \end{aligned} \tag{39}$$

We now have all the elements to obtain the solvability condition of the three equations (31), (32), and (39), relating $\mathcal{D}, (\Pi_+ + \Pi_-)$ and Φ, in terms of $\widehat\lambda = \lambda\tau_{\rm fl}$, $\widehat\omega = \omega\tau_{\rm fl}$ and $\widehat\gamma = \dot\gamma\tau_{\rm fl}$. We obtain the condition

$$\frac{\widehat\lambda}{\widehat\omega}\left(1 - \frac{\widehat\omega - 1}{\widehat\lambda + 1}\right) = \frac{-\zeta}{e^{-\zeta}+1}\frac{(e^{-\kappa_-}-1)(e^{-\kappa_+}-1)}{\kappa_+\kappa_-}\times \times\frac{\kappa_+\sinh\kappa_- - \kappa_-\sinh\kappa_+}{\sinh(\kappa_-) - \sinh(\kappa_+)} \ . \tag{40}$$

The location of the oscillatory instability in the $(\alpha,\widehat\gamma)$ plane, as predicted by the above equation, forms a kind of "bubble" region as shown in Fig. 1. We see that for all $\alpha \in [1/2, \alpha_c]$ where the zero-shear state is unstable, there exists a critical shear-stress $\dot\gamma_c$ beyond which the flow is stabilized and becomes laminar. Conversely, coming from high shear, there is a shear-stress $\dot\gamma_c$ below which the flow becomes intermittent, or stick-slip. This stick-slip phenomenon only exists if the elastic coupling between elements is neither too large, nor too small.

V. NUMERICAL RESULTS

The linear stability analysis derived in the previous sections is in very good agreement with numerical simulations of the model with a discrete number of elements. In order to obtain numerical results we take a set of N elements characterized by continuous stress variables $\{\sigma_i(t)\}_{i=1\cdots N}$ and boolean variables $\{y_i(t)\}_{i=1\cdots N}$ (indicating if the element is jammed or is fluidized). At the beginning of each time step the σ_i of jammed elements are first independently updated by generating Gaussian distributed increments with mean $-\dot\gamma{\rm d}t$ and round mean square $\sqrt{2{\rm d}tD_t}$, where ${\rm d}t$ is a (sufficiently small) discretization time step. All elements for which $|\sigma_i(t)| > \sigma_c$ release their stress with probability ${\rm d}t/\tau_{\rm pl}$, in which case

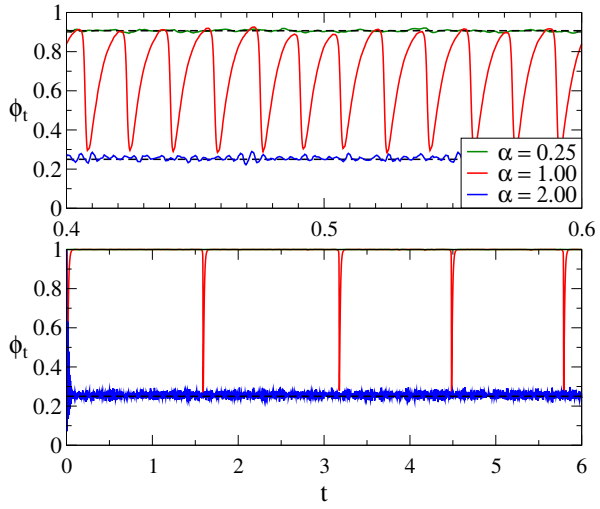

FIG. 2: Fraction of jammed elements versus time for a population of $N = 10^4$ elements undergoing the random walk process described by Eq. (1) (see details in the text) with $\widehat{\gamma} = 0.01$ (top) and $\widehat{\gamma} = 0$ (bottom). Different colors correspond to different values of the coupling constant α (black dashed lines correspond to the analytical stationary solutions in the stable phase). Other parameters are: $\widehat{\omega} = 15$, $D_{\rm i} = 10^{-3}$, $\mathrm{d}t = 10^{-6}$ and $\tau_{\rm pl} = 0$.

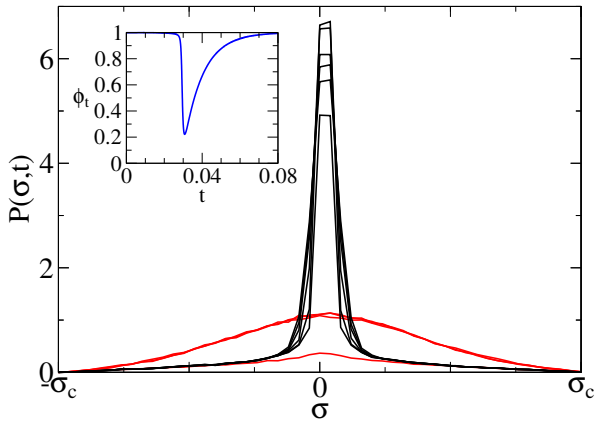

FIG. 3: Empirical distribution of stress variables σ_i for a population of $N = 10^5$ elements with zero shear rate. Different lines are relative to different snapshots taken at equally spaced time intervals of duration 0.01 (the corresponding value for the fraction of jammed elements as a function of time is plotted in the inset). Red lines correspond to the build up of the instability (the lower line is at $t = 0.03$ for example, approximately corresponding to the minimum of $\phi(t)$ in the inset) while black lines correspond to elements progressively relaxing at $\sigma = 0$. For illustrative purposes we set here $\widehat{\gamma} = 0$ while other parameters are: $\alpha = 1$, $\tau_{\rm fl} = 0.01$, $D_{\rm i} = 0.01$, $\mathrm{d}t = 10^{-6}$, $\widehat{\omega} = 30$ and $\tau_{\rm pl} = 0$.

they contribute to the Γ_{t+1} term in Eq. (2) and become fluid. Finally, fluid elements have a probability $\mathrm{d}t/\tau_{\rm fl}$ of being re-activated with stress $\sigma_i = 0$. In the limit of large N the probability $P(\sigma, t)$ of finding a particle with stress between σ and $\sigma + d\sigma$ evolves according to Eq. (1).

In Fig. 2 we plot the fraction of jammed elements ϕ_t versus time for three different values of the coupling constant α with $\widehat{\omega} = 15$, $\tau_{\rm pl} = 0$, $\widehat{\gamma} = 0.01$ (top) and $\widehat{\gamma} = 0$. (bottom). One clearly observes that the liquid and jammed phases are separated by a stick-slip regime for intermediate values of the coupling constant α, as predicted analytically. A more extensive numerical exploration of the model (not shown here) shows a very good agreement with analytical results for the location of phase boundaries depicted in Fig. 1.

In order to have a better understanding of the dynamics of the model in the unstable regime it is instructive to look at the empirical probability distribution $P(\sigma, t)$ at different times corresponding to the accelerated build-up of stress and its subsequent relaxation. This is done in Fig. 3 where we plot the empirical $P(\sigma, t)$ at snapshots equally spaced in time (see the caption for details). We observe that initially, $P(\sigma, t)$ is peaked around zero. Then, as some elements become unstable, the stress diffusion constant increases, bringing more elements close to σ_c. This feedback can become explosive and lead to a "spike" in the number of elements that become unstable simultaneously, see Fig. 3, inset.

Finally, since all the calculations above where made assuming $\tau_{\rm pl} = 0$, we have explored numerically how the instability behaves when $\tau_{\rm pl} > 0$. In this case, we find that the qualitative features of Fig. 1 are left unchanged as long as $\tau_{\rm pl} < \tau^*_{\rm pl}$ where the value of $\tau^*_{\rm pl}$ depends on other parameters, whereas the instability disappears altogether when $\tau_{\rm pl} > \tau^*_{\rm pl}$. For example, in the zero shear rate case, we find for $\widehat{\omega} = 30$ and $\alpha = 2$ that the instability disappears at $\tau^*_{\rm pl} \approx 0.857\ \tau_{\rm fl}$. The reason is quite simple: since jammed elements become unstable at random times with a dispersion $\sim \tau_{\rm pl}$, a large $\tau_{\rm pl}$ maims the synchronisation mechanism that leads to the oscillating instability discovered here. Since the HL model corresponds to $\tau_{\rm pl}/\tau_{\rm fl} \to \infty$, this oscillating instability would not have shown up in the original HL setting. Note that similarly, a small ω (corresponding to a large dispersion in the arrival time of the stress signal) is preventing the instability to occur.

VI. CONCLUSION

In this paper, we have revisited the now classic Hébraud-Lequeux model for the rheology of jammed materials. We have argued that a possibly important time scale is missing from HL's initial specification, namely the characteristic time for a fluidized element to re-jam (chosen to be zero in HL), whose importance has also been stressed in Refs. [18, 20, 32]. A linear stability analysis of the generalized HL model shows that the steady-state solution is in fact unstable for a wide range of parameters, and leads to intermittent, stick-slip flows under a constant shear rate. The stick-slip motion disappears when the shear-rate is large (as expected), or when the time

for a jammed element to become unstable is large compared to the re-jamming time, or else when the elastic coupling between jammed elements is either too weak or too strong (see Fig. 1 above).

The instability we find is akin to the synchronization transition of coupled elements that arises in many different contexts (neurons, fireflies, financial bankruptcies, etc.), see [30, 31] and references therein. Similar instabilities are found in some variants of the SGR models [27] and within simple phenomenological constitutive equations for shear-thickening materials [28], although the underlying physical mechanism does not seem to be related to the synchronisation effect discussed here. We hope that our scenario could shed light on the commonly observed intermittent, serrated flows of glassy materials under shear. It would also be quite interesting to study our instability in finite dimensions (rather than in the HL mean-field limit), and along the lines recently suggested by Lin and Wyart [25], where the HL diffusion term is replaced by a long-range, Lévy flight diffusion. It is not immediately clear whether the stick-slip instability survives such a deep modification of the mathematical and physical nature of the model.

Acknowledgments

The authors would like to thank J.-L. Barrat, M. E. Cates, A. Rosso, and M. Wyart for many stimulating discussions and remarks concerning this work.

[1] J.-C. Baret, D. Vandembroucq, and S. Roux, Phys. Rev. Lett. **89**, 195506 (2002).
[2] M. Otsuki and H. Hayakawa, Phys.Rev.E **90**, 042202 (2014).
[3] K. Chen, P. Bak, and S. Obukhov, Phys. Rev. A **43**, 625 (1991).
[4] E. Lerner, G. Dring, and M. Wyart, Europhysics Letters **99**, 58003 (2012).
[5] A. Argon, Acta Metallurgica **27**, 47 (1979).
[6] H. Princen, Journal of Colloid and Interface Science **91**, 160 (1983).
[7] M. Falk and J. Langer, Phys. Rev. E **57**, 7192 (1998).
[8] J. Langer, Phys. Rev. E **77**, 021502 (2008).
[9] P. Schall, D. A. Weitz, and F. Spaepen, Science **318**, 1895 (2007).
[10] S. Manneville, L. Bécu, and A. Colin, European Physical Journal Applied Physics **28**, 361 (2004).
[11] A. Amon, V. B. Nguyen, A. Bruand, J. Crassous, and E. Clément, Phys. Rev. Lett. **108**, 135502 (2012).
[12] C. E. Maloney and A. Lemaître, Phys. Rev. E **74**, 016118 (2006).
[13] A. Tanguy, F. Leonforte, and J.-L. Barrat, Eur. Phys. J. E **20**, 355 (2006).
[14] G. Picard, A. Agdari, F. Lequeux, and L. Boquet, Eur. Phys. J. E **15**, 371 (2004).
[15] P. Hébraud and F. Lequeux, Phys. Rev. Lett. **81**, 2934 (1998).
[16] P. Sollich, F. Lequeux, P. Hébraud, and M. E. Cates, Phys. Rev. Lett. **78**, 2020 (1997).
[17] P. Sollich, in *Molecular Gels* (Springer, 2006), pp. 161–192.
[18] E. Jagla, F. P. Landes, and A. Rosso, Phys. Rev. Lett. **112**, 174301 (2014).
[19] C. K. Lieou, A. E. Elbanna, J. Langer, and J. Carlson, `arXiv:1506.00331` (2015).
[20] P. Coussot and G. Overlez, Eur. Phys. J. E **33**, 183 (2010).
[21] D. Rodney, A. Tanguy, and D. Vandembroucq, Modelling Simul. Mater. Sci. Eng. **19**, 083001 (2011).
[22] W. H. Herschel and R. Bulkley, Kolloid-Zeitschrift **39**, 291 (1926).
[23] E. Agoritsas, E. Bertin, K. Martens, and J.-L. Barrat, Eur. Phys. J. E **38**, 71 (2015).
[24] E. Jagla, `arXiv:1506.01005` (2015).
[25] J. Lin and M. Wyart, `arXiv:1506.03639` (2015).
[26] A. Lemaître and C. Caroli, `arXiv:0705.3122` (2007).
[27] D. A. Head, A. Ajdari, and M. E. Cates, Phys. Rev. E **64**, 061509 (2001).
[28] A. Aradian and M. E. Cates, Phys. Rev. E **73**, 041508 (2006).
[29] S. Gualdi, M. Tarzia, F. Zamponi, and J.-P. Bouchaud, Journal of Economic Dynamics and Control **50**, 29 (2015).
[30] S. Gualdi, J.-P. Bouchaud, G. Cencetti, M. Tarzia, and F. Zamponi, Phys. Rev. Lett. **114**, 088701 (2015).
[31] S. Strogatz, *Sync: The emerging science of spontaneous order* (Hyperion, 2003).
[32] K. Martens, L. Bocquet, and J.-L. Barrat, Soft Matter **8**, 4197 (2012).
[33] F. Puosi, J. Olivier, and K. Martens, `arXiv:1501.04574` (2015).